48th AIAA Aerospace Sciences Meeting Including the New Horizons Forum and Aerospace Exposition
4 - 7 January 2010, Orlando, Florida
AIAA 2010-964

Investigation of Impedance Characteristics and Power Delivery for Dielectric Barrier Discharge Plasma Actuators

Justin C. Zito[1] and David P. Arnold[2]
Interdisciplinary Microsystems Group, Department of Electrical and Computer Engineering, University of Florida, Gainesville, FL 32611-6200

Ryan J. Durscher[3] and Subrata Roy[4]
Computational Plasma Dynamics and Test Facility, Mechanical and Aerospace Engineering Department, University of Florida, Gainesville, FL 32611-6300

Dielectric barrier discharge (DBD) plasma actuators have received recent attention for various flow-control applications. To enable system-level design and optimization of plasma actuator systems—including the actuators and all power electronics—equivalent electrical circuit models of the plasma actuators are desired. To address this need, the current/voltage/power behaviors of different DBD plasma actuators designs are experimentally characterized under sinusoidal electrical excitation at varying amplitudes (4 – 10 kV_{pk}) and frequencies (10 – 20 kHz). A simplified parallel resistor–capacitor circuit is used to model the behavioral electrical impedance of the actuators. The dependencies of the circuit model parameters are studied as functions of actuator geometry, excitation amplitude, and excitation frequency. Based on this analysis, considerations for electrical impedance load matching are discussed.

Nomenclature

A_L	=	load impedance vector magnitude, Ω
C	=	matching network capacitance, F
C_p	=	plasma actuator effective load capacitance, pF
d	=	thickness of dielectric substrate, mm
f	=	frequency of input signal, kHz
g	=	gap distance between electrodes, mm
l	=	length of electrode, cm
L	=	matching network inductance, H
P_{avg}	=	average power delivered to load, W
R	=	dc resistance of matching inductor, Ω
R_L	=	load impedance resistance, Ω
R_S	=	source impedance resistance, Ω

[1] Graduate Student, Student Member AIAA, jcz@ufl.edu.
[2] Assistant Professor, Member AIAA, darnold@ufl.edu.
[3] Graduate Student, Student Member AIAA, dursch@ufl.edu.
[4] Associate Professor, Associate Fellow AIAA, roy@ufl.edu.

R_p = plasma actuator effective load resistance, MΩ
V_{pk} = peak amplitude of oscillation, kV
w = width of electrode, cm
X_L = load impedance reactance, Ω
X_S = source impedance reactance, Ω
Z_L = complex load impedance, Ω
Z_S = complex source impedance, Ω
ϕ_L = load impedance phase angle, degrees
ω = radian frequency ($2\pi f$), rad/s

I. Introduction

DIELECTRIC barrier discharge (DBD) plasma actuators are gaining popularity for various applications within the field of active flow control, including boundary layer modification, lift augmentation, and separation control over a variety of airfoils/surfaces.[1] A schematic of a typical DBD plasma actuator is shown in Figure 1. There are two strip-like electrodes separated by a dielectric material of thickness *d*. The electrodes are connected to a high-voltage power supply, with the bottom electrode grounded. When a high-voltage ac voltage signal is applied to the top electrode, the fluid, in this case air, weakly ionizes in the local vicinity. This results in an electrohydrodynamic (EHD) body force imparted on the fluid near the dielectric surface. The electrodes are often offset by distance *g* to extend the electric field and create a wider plasma discharge. Creating a larger area of plasma provides favorable effects on the velocity and forces attainable with these actuators. This however requires a higher power demand on the power supply.

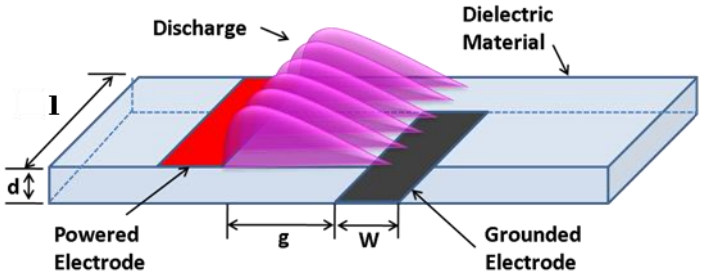

Figure 1. Configuration of the DBD plasma actuator, shown with gapped electrodes.

The power supplies used in most plasma actuation experiments employ large, bench-top amplifiers and/or one or more transformers to generate the high-voltages (kilovolts) required for DBD actuators. For future system integration on flight vehicles, the size and mass of the power system is of great importance. For design purposes, it is assumed that maximum fluidic impact of a plasma actuator is achieved by maximizing the real power delivered to the actuator. Thus, the ultimate circuit design goal is to maximize the power transfer from the power supply to the load (actuator).

In electrical circuit design, maximum power transfer is achieved by "matching" the source and load impedances, where the load impedance Z_L (plasma actuator) is designed to be the complex conjugate of the source impedance Z_S (power supply), i.e. $Z_L = R_L + jX_L = Z_S^* = R_S - jX_S$. In this case, the power supply size and wiring requirements are minimized. In order to

exactly match the source and load impedances, it requires that the reactive components cancel (jX_L = - jX_S) and the resistive components are equal (R_L = R_S). As will be shown later, the effective load resistance R_L of a plasma actuator is often very high (MΩ – GΩ range). Complete matching would thus require a power supply with a very high output impedance, which is not common. As a result, complete matching may not be possible. In this case, the load can be partially matched by ignoring the mismatch between the resistive components and focusing on canceling the reactive component. In this situation the reactive power (power reflected back and forth between the source and load) is minimized.

Since the design of particular plasma actuator and power supply may not facilitate a natural impedance match, a load-matching network may be required between the power supply and actuator load.[2] Load-matching networks are well-documented for power electronic and RF systems.[3,4] However, DBD plasma actuator loads present complications because the plasma generation is both non-linear and time-varying. First, the timescale of generation and recombination of the ions is short compared to the time period of the driving signal; this creates current spikes in the observed waveforms. Second, the apparent impedance changes depending on the driving amplitude and frequency. These effects complicate the ability to realize impedance matching networks, especially if the driving amplitude and frequency change with time, as may be the case for plasma actuators used on future flight vehicles.

To address these challenges, an experimental study to extract the load characteristics of different DBD plasma actuators under varying amplitudes and frequencies is performed. In addition to voltage, current, and power measurements, a simple resistor-capacitor impedance model is used to characterize the dominant electrical impedance of the plasma actuator load. Experiments are performed using copper electrodes on a 0.20-cm-thick polymethyl methacrylate (PMMA) as the dielectric substrate. PMMA is an acrylic material with a dielectric strength of 25 MV/m and good uniformity. The dielectric strength and uniformity prevent arcing between the electrodes, making PMMA an effective and reliable dielectric material for the plasma discharge.

Two sets of experiments were conducted. In the first set of experiments, comparisons are made between un-gapped and gapped actuators (g = 3 mm), where the electrode length is 10 cm in both cases. A second set of experiments studies trends as the length of un-gapped actuator electrodes vary from 5 – 20 cm. The goal of these efforts is to provide an understanding of the impedance behavior of DBD actuator designs under various electrical excitations. This information will help facilitate future efforts for maximizing energy transfer to the load via load matching or other techniques.

II. Experimental Methods

1. Experimental Setup

As shown in Figure 2, the power supply for a DBD plasma actuator consists of a function generator, an amplifier, and a transformer providing a high-voltage sinusoidal signal to the load. For the experiments presented here, the load characteristics were the primary focus; the performance of the power source (amplifier, transformer) and net power delivery system were not studied. Thus, the voltage and current of the actuator load were monitored by direct electrical measurements at the terminals of the plasma actuators. A Pearson current monitor (model 2100) was used to measure the current at the input to the actuator load, and a Tektronix high-voltage probe (model P6015A) measured the potential across the load. A digitizing oscilloscope (Tektronix DPO 3054) was used to capture and record the measured signals for post-processing in MATLAB. Details of the data acquisition are provided in sub-section 4.

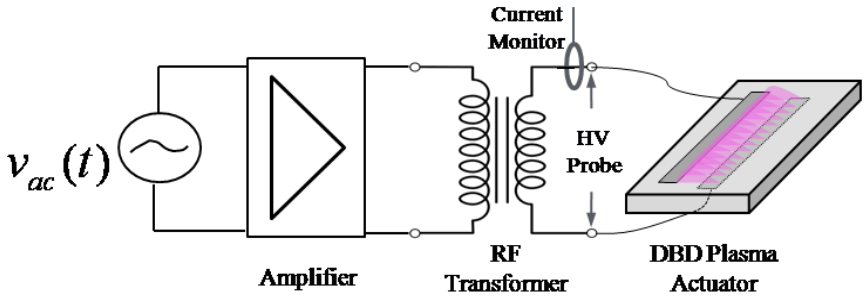

Figure 2. Schematic of DBD Plasma Actuator; from left to right: source signal (function generator), amplifier, transformer, and plasma actuator. The high-voltage probe and current monitor capture the waveforms at the inputs to the actuator terminals.

2. Voltage-Current-Power Relationships

It has been previously determined that the plasma discharge is mostly influenced during the positive slope of the driving voltage waveform.[5,6] To better understand this effect, representative current, voltage, and instantaneous power waveforms are plotted in Fig. 3a for the gapped (g = 3 mm) actuator at 14 kHz and 8 kV_{pk} voltage amplitude. The instantaneous power was computed via point-by-point multiplication of the voltage and current data values.

Many interesting effects can be observed from the plots. First, the high-voltage waveform delivered to the load is seen to be fairly sinusoidal in shape. In contrast, the current waveform has a general sinusoidal shape, but with a series of high-amplitude spikes, predominately during the rising voltage waveforms. This indicates different time scales: a long time-scale (~100 μs) associated with the sinusoidal waveforms and a shorter time-scale (~1 μs) associated with the spikes, presumably from conductive current discharges through the plasma. Second, the current and voltage signals are roughly 90° out of phase, with the current leading the voltage. This indicates a strongly capacitive load, since for an ideal capacitive load the current would lead the voltage by exactly 90°.

Focusing now on Fig. 3b, the power waveform exhibits twice the frequency of the current and voltage signals, resulting from the multiplication of the sinusoidal voltage and current signals. The instantaneous power indicates the power flowing into or out of the load. When this value is positive (whenever the current and voltage have the same polarity), power is flowing into the load; when negative, power is flowing out of the load. The measured waveforms show positive power delivery on both the positive and negative half-cycles. For example during the positive half-cycle, as the voltage rises, the power rises (along with spikes), but as the voltage falls, power flows back out of the load. A similar effect is seen for the negative half-cycle. This reversible "sloshing" of power into and out of the load is characteristic of reactive load impedance (as opposed to resistive). Much of this reversible energy transfer is attributed to reversible potential energy storage in the electric fields of the actuator. As mentioned previously, it is assumed that this reactive power flow is not contributing to plasma formation, so it should be minimized through appropriate impedance matching.

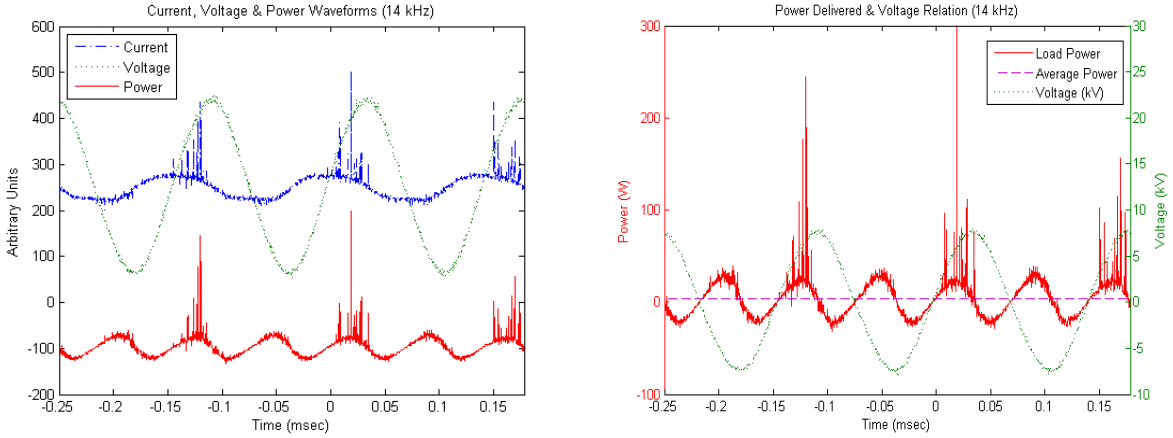

Figure 3. (a) Time waveforms of voltage, current, and instantaneous power signals (note: arbitrary amplitudes); (b) Voltage and power waveforms showing that the majority of power is delivered during the increasing half-cycle (positive slope) of the voltage waveform.

The plots show the instantaneous power transfer, but the *average* power delivered to the load is more practically relevant, since irreversible energy transfer to the fluid is assumed necessary for flow interaction (e.g. to enact work on the flow). Mathematically, the average real power is simply the time-average value of the instantaneous power waveform,

$$P_{avg} = \frac{1}{nT}\int_0^{nT} v(t)\,i(t)\,dt, \tag{1}$$

where $v(t)$ and $i(t)$ are the voltage and current time-waveforms, respectively; T is the oscillation period; and n is the number of periods over which the average is computed. In the case here, irreversible power transfer occurs primarily as a result of the current/power spikes. The instantaneous positive power contributions from these spikes increase the average power; otherwise the power signal would oscillate around zero, yielding an average power transfer of zero.

As reported by other groups,[5,6] there are larger spikes on the rising edge of the positive voltage half-cycle and smaller spikes on the falling-edge of the negative voltage half-cycle. Real power is being delivered in both cases, but the positive and negative voltage half-cycles do not contribute power equally. For the waveforms shown in Fig. 4, instantaneous power spikes in excess of 300 W were measured, but the average power delivered is only 3.9 W, the majority occurring during the positive voltage half-cycle. Methods to maximize power transfer in both half-cycles remains an open area for investigation.

3. Impedance Model and Experimental Extraction

Following from the previous section, the long-time-scale voltage/current/power waveforms observed for DBD actuators exhibit a reactive (capacitive) impedance behavior, but the short-duration spikes clearly result in net power transfer. Thus, the load is both reactive and resistive. The next step is to model this behavior with an appropriate circuit model. The goal is to capture

the effective impedance behavior over one or more time cycles, not necessarily the short-time-scale dynamics of the plasma discharge.

Based on the observed voltage-current behavior, the actuator impedance is modeled by a parallel-connected resistor R_p and capacitor C_p, as shown in Fig. 4. The capacitor is intended to model the reactive behavior, while the resistor is used to model the real power delivered to the load. More complicated circuit models have been proposed to better describe the phenomenological physics,[7,8] but these can usually be simplified via circuit analysis to a simple RC-network.[2]

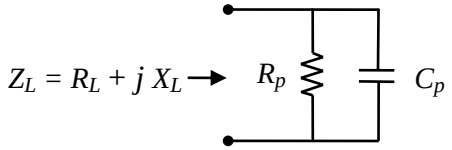

Figure 4. Equivalent circuit representation of plasma actuator load.

The input impedance, Z_L, of this parallel RC network in rectangular coordinates is

$$Z_L = R_L + jX_L \tag{2}$$

where the real and imaginary impedances are

$$R_L = \frac{R_p}{1+\omega^2 R_p^2 C_p^2}, \tag{3}$$

$$X_L = \frac{-\omega R_p^2 C_p}{1+\omega^2 R_p^2 C_p^2}. \tag{4}$$

The input impedance can also be represented in polar coordinates as

$$Z_L = A_L \angle \phi_L \tag{5}$$

with magnitude and phase

$$A_L = \sqrt{R_L^2 + X_L^2} = \frac{\sqrt{R_p^2 + \left(\omega R_p^2 C_p\right)^2}}{1+\omega^2 R_p^2 C_p^2}, \tag{6}$$

$$\phi_L = \tan^{-1}\left(\frac{X_L}{R_L}\right) = \tan^{-1}\left(-\omega R_p C_p\right). \tag{7}$$

The relationships between the rectangular and polar representations are shown graphically in Fig. 5.

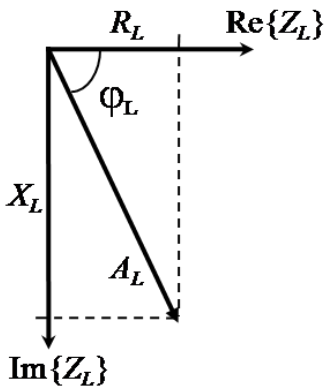

Figure 5: Graphic representation of the DBD plasma load impedance.

Impedance analysis and extraction of R_p and C_p for a linear RC electrical load is straightforward. The load impedance can be directly calculated based on the relative magnitude and phase of the current and voltage waveforms. For a DBD actuator, the current waveform is clearly not a pure sinusoid; rather it is highly nonlinear and "noisy." This complicates the signal analysis. Despite this, a method is proposed below to extract an effective impedance from the experimentally measured data. The basic idea is to use the phase shift between the fundamental sinusoidal current/voltage waveforms to determine the phase angle ϕ_L, and use the average real power delivered to the load to determine the effective plasma load resistance R_P. From these two values, the effective plasma load capacitance C_p can be found. The methods for experimentally extracting these values are described below.

The voltage waveform is assumed perfectly sinusoidal, yielding the relationship

$$R_P = \frac{V_{rms}^2}{P_{avg}} = \frac{V_{pk}^2}{2P_{avg}}, \tag{8}$$

from which R_p is calculated. The peak amplitude of the voltage signal is directly measured using the oscilloscope, and the average power is calculated by Eq. (1), computed over n periods.

Determination of the phase angle ϕ_L is more difficult, because of distortion in the current waveform. A non-linear least squares approximation method is used to fit sinusoidal curves to both the voltage and current waveforms. The relative phase between the two fitted curves is then used to compute the relative phase angle ϕ_L, also computed over n cycles. Figure 6 shows an example of raw current data and the resulting curve fit. In general, the spikes in the current waveforms affect the fit in amplitude, but not the phase. Since only the phase information is important for extraction of ϕ_L, any error in amplitude is not of great concern.

Once R_p and ϕ_L are found, the load capacitance C_p is calculated following from Eqns. (2) – (8):

$$C_p = \frac{\tan\phi_L}{\omega R_P}. \tag{9}$$

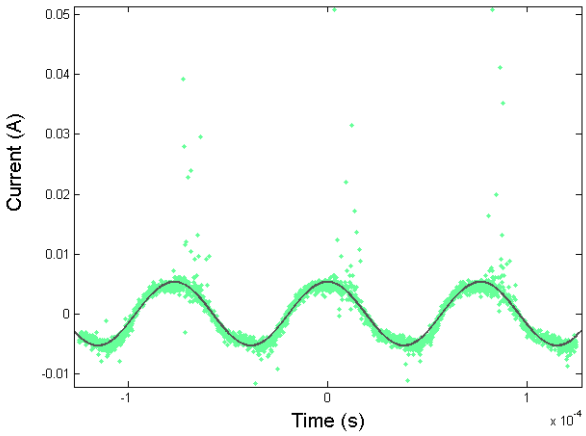

Figure 6. Current waveform data shown with curve fit using non-linear least squares method.

4. Data Acquisition

Preliminary experiments indicted the extracted parameters exhibited relatively strong dependencies on the data acquisition parameters. For example, changing either the sampling rate and/or the total number of samples yielded varying results in the load power computation. Sampling only a few periods worth of data resulted in variations in the average load power that deviated up to 10 % among identical experiments. Increasing the measured data record to 30 or more periods reduced the measurement uncertainty of the average power below 0.2 %. Increasing the sampling rate from 5 up to 250 MSa/s (M- samples per second), however, did not have any substantial impact in reducing the uncertainty in the mean power. For all of the results presented in this paper, three trials were used for each test. Each trial was sampled at 250 MSa/s with one million samples captured, resulting in 40 – 56 measured periods per trial depending on the input frequency.

Another consideration is the bandwidth limitation of the current probe. The bandwidth of the Pearson 2100 current probe is 20 MHz. When sampling faster than 20 MSa/s, the measured current waveform indicated a transient ringing effect following each individual current spike. The oscilloscope had the ability to apply a bandwidth limit on individual channels. Setting the bandwidth limit to 20 MHz for the current signal corrected this problem.

III. Results

In the first set of experiments, two DBD actuator geometries were used, as shown in Fig. 7. The electrodes were made from 10 cm long x 0.5 cm wide x 0.013 cm thick adhesively backed copper tape. One of the geometries had a lateral gap between the two electrodes (g = 3 mm), while the other had no gap (g = 0 mm). The dielectric substrate was the same for both actuators, made from 0.20 cm thick PMMA.

Using these two actuators, two parametric tests were conducted using sinusoidal waveforms. In the first, the amplitude of the ac voltage input signal was varied in 0.5 kV increments, while the frequency was held constant at 14 kHz. The actuator with no gap was tested at amplitudes ranging from 4.5 – 9 kV_{pk}, while the actuator with the 3 mm gap was tested at amplitudes from 6 – 9 kV_{pk}. The gapped design required higher initial voltage amplitude to create sufficient

electric field for uniform plasma discharge. In the second parametric test, the frequency was varied from 10 to 17 kHz, while the voltage amplitude was fixed at 8 kV_{pk} for both the gapped and un-gapped geometries.

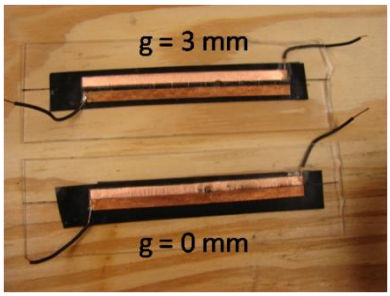

Figure 7. Two actuator geometries are shown for the electrode gap experiment; top actuator has a 3 mm gap and the bottom has zero gap.

In the second set of experiments, an un-gapped (g = 0 mm) geometry was tested using four different electrode lengths to characterize the trends as the input amplitude was varied. The basic construction was similar to the previous tests: electrodes were 0.5 cm wide x 0.013 cm thick adhesively backed copper tape, and the substrate was 0.20 cm thick PMMA. The first test was conducted using 20 cm long copper electrodes. The electrodes were then shortened by 5 cm and tested again, and this was repeated in order to test 20, 15, 10 and 5 cm long actuators. Figure 8 shows the four actuators with different electrode lengths. In each case, the actuator was tested at 14 kHz with amplitudes ranging from 4.5 – 8.5 kV_{pk}.

Figure 8. Experimental setup showing the four different electrode lengths tested; From left to right: 20, 15, 10 and 5 cm long actuators (0.5 cm wide, zero gap).

1. Power Consumption

The average power delivery for the 0 and 3 mm gap actuators was measured over a range of frequencies and amplitudes, as shown in Fig. 9. The average power consumption grows with both increasing amplitude and frequency, with a larger dependence on the amplitude. The data indicates that for the same drive voltage amplitude and frequency, more power is delivered to the un-gapped (g = 0 mm) actuator, indicating a different input impedance. Presumably, with a smaller inter-electrode gap, the electric field is stronger, creating more ionization.

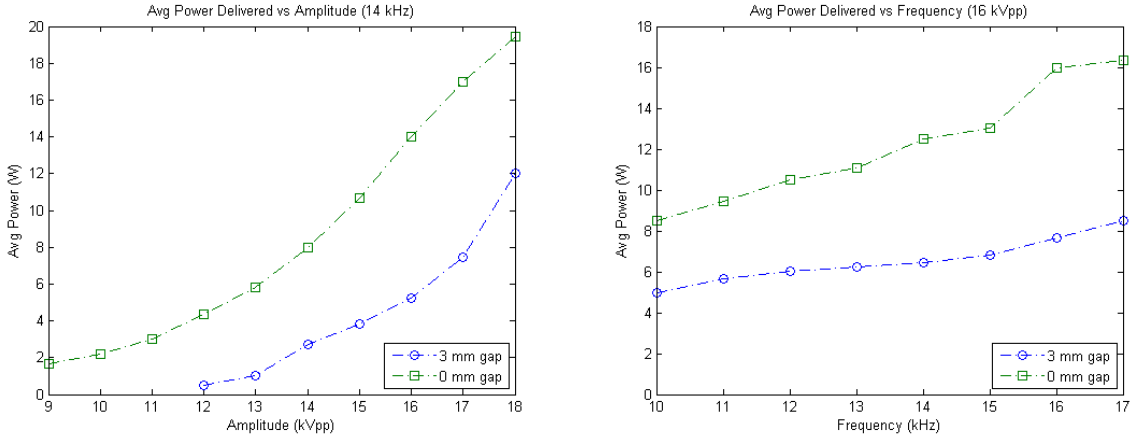

Figure 9. Average power delivered to the DBD plasma load for the gapped and un-gapped design with (a) varying amplitude and (b) varying frequency.

The electrode length test shows similar trends to the data from the electrode gap data. The average real power delivered to the load is plotted in Figure 10 against varying input amplitudes for each of the actuators tested. In this case, the power is normalized by the actuator length to enable comparison of the amount of power consumed for the different electrode lengths. Since the curves collapse on one another, the results indicate that the total power scales proportional to the electrode length. In a practical system, this indicates there may be no difference whether powering several short actuators vs. one long actuator. As before, however, more power is required at higher excitation voltages.

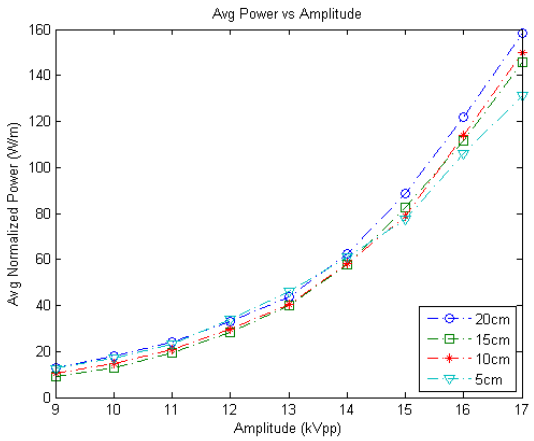

Figure 10. Average normalized power delivered to the plasma with varying amplitude for each test case.

2. Electrical Impedance Data

Following the previously described procedures for data extraction, the magnitude A_L and phase ϕ_L of the plasma load impedance are plotted against both amplitude and frequency in Fig. 11 for the electrode gap experiment. With increasing voltage amplitude (Fig. 11a), the total

magnitude of impedance decreases steadily (note the log scale on the y-axis), and the phase decreases fairly linearly from ~86° down to 71°. With increasing frequency (Fig. 11b), the magnitude of the impedance decreases only slightly, and the phase remains fairly constant around 77°. From these results, the apparent load impedance is indeed affected by the applied input voltage amplitude, and to a lesser degree, the frequency.

The impedance data is translated into equivalent circuit model parameters R_p and C_p, following Eqns. (8) – (9). These values are plotted in Fig. 12 as functions of amplitude and frequency. Here, some interesting trends are observed. With increasing amplitude (Fig. 12a), the effective resistance decreases, presumably from more ionization and a better conduction path. At the same time, the effective capacitance increases, indicating more potential energy storage. The resistance and capacitance show a weaker yet similar dependence upon frequency (Fig. 12b). For both types of actuators, the resistance gradually decreases from 10 – 17 kHz, and the capacitance remains nearly constant over that frequency range.

Common data points to the "vs. amplitude" and "vs. frequency" plots are circled in the figures. For the zero-gap actuator at 8 kV_{pk}, the effective resistance and capacitance are quite similar, ~8 MΩ and ~8 pF, respectively. Similarly, for the 3 mm gap actuator at 8 kV_{pk}, the effective resistance and capacitance are in agreement between the two tests, ~10 MΩ and ~5 pF, respectively.

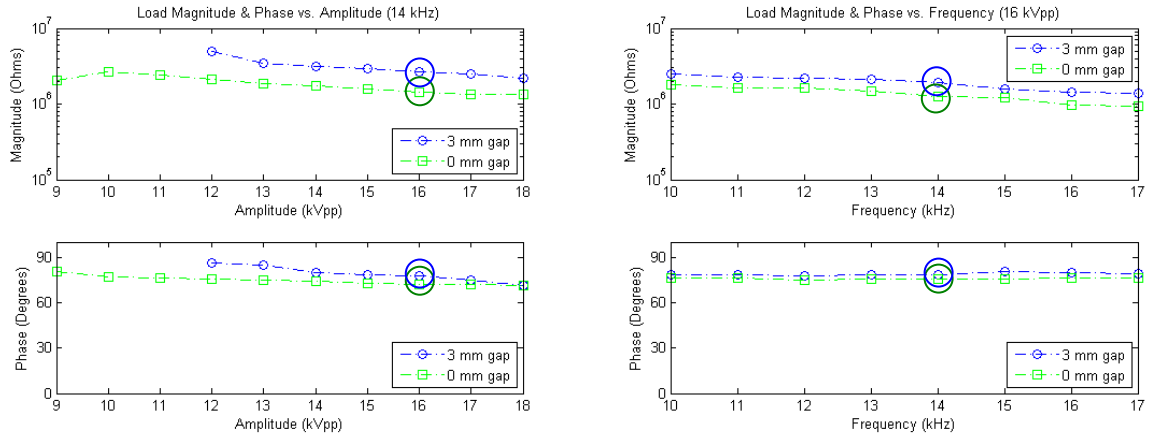

Figure 11. Effective magnitude A_L and phase ϕ_L of plasma load impedance with (a) varying amplitude and (b) varying frequency. Data points common to both figures are circled for emphasis.

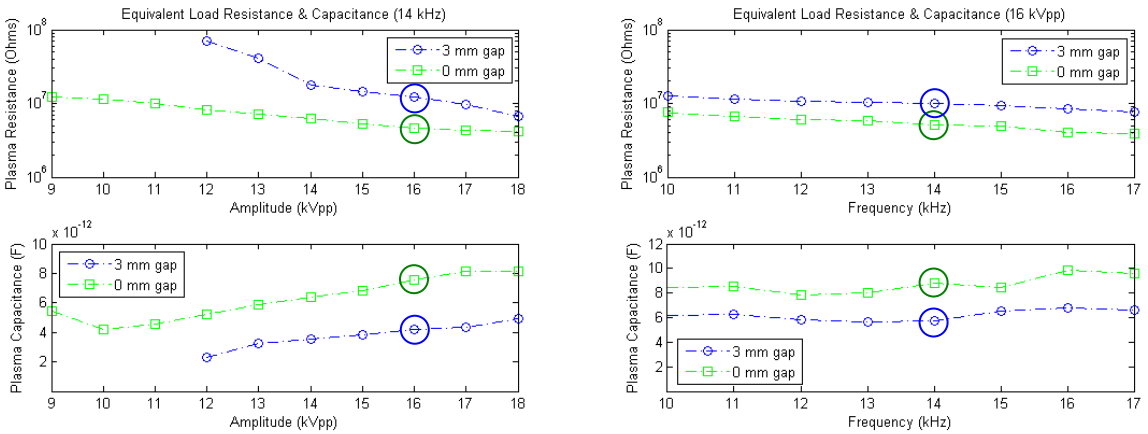

Figure 12. Effective parallel resistance *Rp* and capacitance *Cp* of plasma load with (a) varying amplitude and (b) varying frequency. Data points common to both figures are circled for emphasis.

The same parameter extraction methods were used to compute the magnitude and phase, as well as the effective load resistance and capacitance, for the varying electrode length tests. These results are plotted in Figures 13 and 14. From Figure 13, the magnitude of the load impedance decreases steadily within the MΩ range, similar to the trend observed in the previous experiment. The phase also follows a similar trend, decreasing roughly linearly from just above 80^o to ~ 70^o.

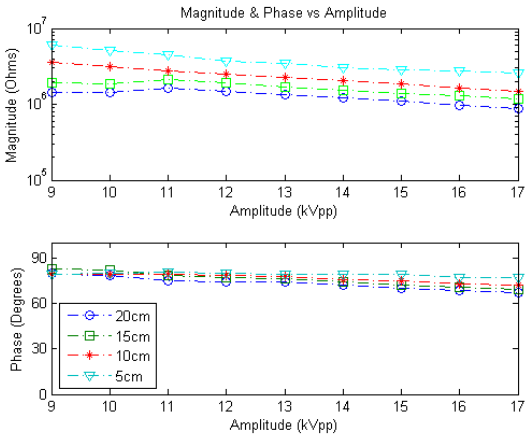

Figure 13. Effective magnitude A_L and phase ϕ_L of plasma load impedance with varying amplitude.

From Figure 14, it can be seen that the effective load capacitance increases with amplitude, again following the previous experimental results. The capacitance also increases with increased electrode length, which may be intuitively expected, as the area of the plasma load 'capacitor' is also increased. The plasma resistance decreases with increased amplitude, and also with increased electrode length. This is evidence of an increased conduction path. The trends for both effective capacitance and resistance scale roughly proportional to the actuator length, i.e.

doubling the actuator length results in twice the capacitance and half the resistance, at least under the various excitation conditions studied here.

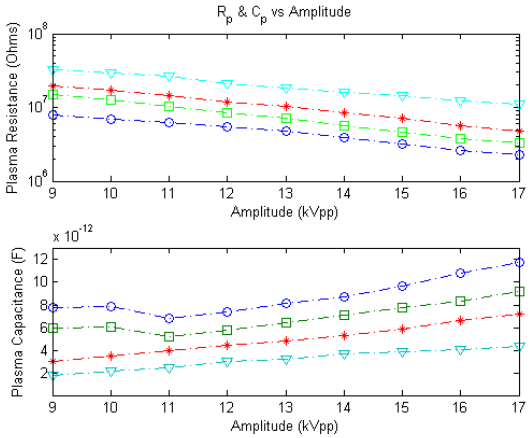

Figure 14. Effective parallel resistance *Rp* and capacitance *Cp* of plasma load with varying amplitude.

Comparing the data from the two different sets of experiments, there is also reasonable agreement. Theoretically, the data from the 10 cm long electrode in this experiment data set should match the data from the actuator with zero-gap in the electrode gap test. The geometries of both actuators are 10 cm long x 0.5 cm wide with zero-gap. At 8 kV_{pk} amplitude, the 10 cm long electrode exhibits an equivalent resistance of ~6 MΩ and ~7 pF. This is similar to the values from the equivalent zero-gap electrode test (~8 MΩ and ~8 pF). The overall range of resistance and capacitance values for the various actuator geometries are in the range of 2 – 30 MΩ, and 2 – 12 pF, respectively.

IV. Considerations for Impedance Matching

With an understanding of the impedance characteristics of the DBD actuator load, the next step in system design would be to optimize the power transfer from the power supply to the plasma actuator load, while minimizing the power dissipated in the interconnecting circuitry. As shown previously, a reactive load results in unwanted oscillating power flow into and out of the load. This oscillatory reactive power flow does not contribute net average real power to the load, so power systems often include matching networks to counteract this effect. The purpose of the matching network is to counteract the reactive (in this case capacitive) nature of the plasma actuator, so that the power supply "sees" a purely resistive load. This can be achieved using various electrical networks.

1. Motivation for Impedance Matching

The need for impedance matching may not be clear until looking at the amount of real power that is delivered to the load in comparison to the total amount of available power within the circuit. The power factor, *pf*, of an electrical load is defined as the ratio of the real power *P* consumed at the load to the apparent power |*S*|

$$pf = \frac{P}{|S|}. \tag{12}$$

The power factor varies between zero and one, with one being the ideal value (no reactive power; all real power). The power factor can be calculated from the phase angle of the load impedance as

$$pf = \cos(\phi_L) = \frac{R_L}{\sqrt{R_L^2 + X_L^2}}. \tag{13}$$

The power factor gives some idea of how much power within the system is used effectively, as the reactive component of the power is purely imaginary and has no contribution to the plasma discharge. Figure 16 visualizes a plot of the power factor for the gapped electrode tests. The maximum power factor is around 0.3, indicating that there is a 70 % overhead in the power system (only 30% of the apparent power is real power delivered to the load). At lower input voltages, the power factor is below 0.2, indicating even worse transfer of real power to the DBD plasma actuator.

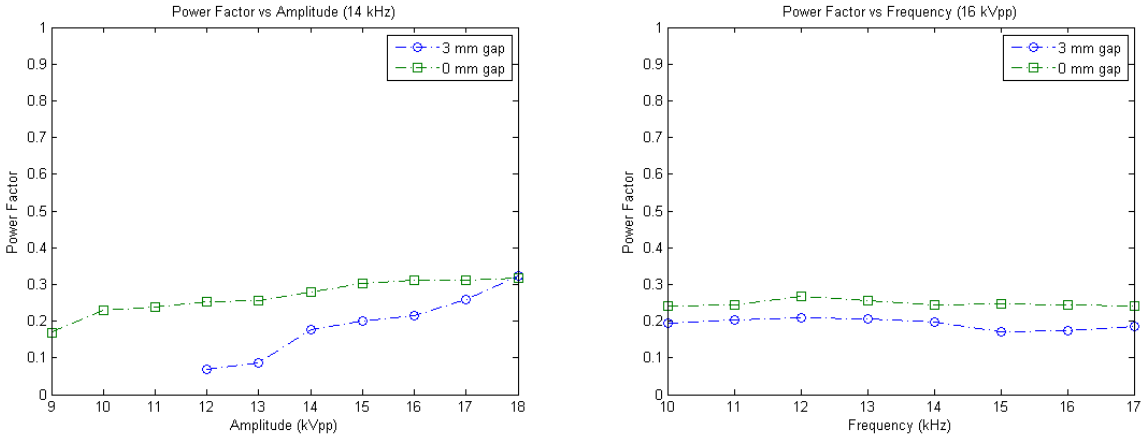

Figure 16. Power factor plotted against varying amplitude (left) and varying frequency (right).

The power factor for the electrode length varying experiment is shown in Figure 17. The power factor is nearly 20 % at 9 kV_{pp} amplitude and increases just over 30 % at 18 kV_{pp}. The data implies that the power factor is higher for the longer electrodes, indicating that the longer plasma actuator loads are less reactive. This data hopefully gives clear motivation of the need for impedance matching between the power supply and plasma load.

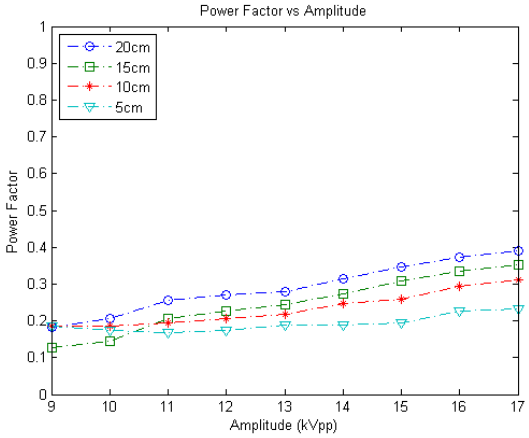

Figure 17. Power factor plotted against amplitude for the actuators with varying electrode lengths.

2. Impedance Matching Example

Following the work of Chen[2] et al., an all-shunt impedance matching circuit is considered for impedance matching on the secondary side (high-voltage side) of the transformer. This impedance matching uses a capacitor and inductor placed in parallel with the actuator load. An equivalent model for the plasma actuator and load matching circuit is shown in Figure 14. The resistance R in series with the matching inductor is included to account for the DC resistance associated with the inductor.

The total impedance of the matching network and plasma load is given by

$$Z_{tot} = R_{tot} + jX_{tot} = (R + j\omega L) \| \frac{1}{j\omega(C + C_p)} \| R_p \,. \tag{10}$$

Impedance matching is highly dependent on the signal frequency, as the impedance values of the matching inductor and capacitor are also functions of the signal frequency (recall $X_C = (j\omega C)^{-1}$ and $X_L = j\omega L$). Thus, ideal impedance matching only occurs at one specific frequency. In practice, the desired operating frequency is first selected, and then matching component values are calculated so as to force the reactive (imaginary) impedance component, X_{tot}, to zero. The matching frequency, as a function of the matching components and the load reactive component (C_p), is given by[2]

$$\omega_0 = \sqrt{\frac{1}{L(C + C_p)} - \frac{R^2}{L^2}} \,. \tag{11}$$

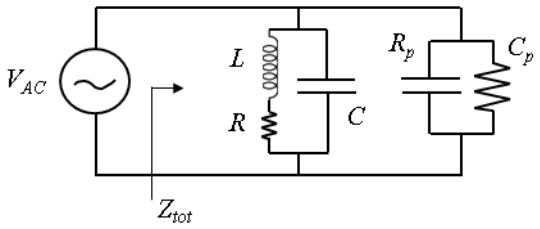

Figure 14. Circuit model; the shunt matching network is connected in parallel with the plasma load model (R_p and C_p).

Consider possible impedance matching component values for an actuator with 10 cm long electrodes, with C_p = 5 pF, operating at 14 kHz. The R value depends on the inductor, and varies among different manufacturers. For the frequencies of interest, ω_o^2 is usually much larger than typical inductor component values of $(R/L)^2$. Therefore the R/L term in (11) can be ignored. Based on this, Table 1 summarizes some possible impedance matching values. Matching with only an inductor and no capacitor would require a 25.8 H inductance, an impractically large value. However, as the matching capacitance increases into the nano- to micro-farad range, the required matching inductance becomes smaller and within reasonable physical values. It should be highlighted that any inductor and capacitor used must be able to withstand the high voltages applied to the actuator load, since the components are in parallel.

C	*L*
0 F	25.8 H
1 pF	21.5 H
10 pF	8.6 H
100 pF	1.2 H
10 nF	13 mH
0.1 μF	1.3 mH
10 μF	13 μH
100 μF	1.3 μH
500 μF	258 nH
1 mF	130 nH

Table 1. Projected values for matched impedance at 14 kHz for a 10 cm long actuator with an equivalent plasma capacitance of 5 pF.

V. Conclusions

This paper studies the impedance characteristics of DBD plasma actuators having several different geometries. Examination of the electrical impedance of various DBD actuators under different sinusoidal excitation reveals a predominately capacitive behavior. The actuators exhibit a diode-like nonlinear conduction behavior, where the resistance is very high above a certain

threshold voltage value. Once the voltage exceeds that required to generate the plasma discharge, the resistance decreases as the conduction path is established for current flow.

A method is presented for modeling the actuator load with a parallel resistor/capacitor electrical model. For the actuators and excitation levels explored here, the equivalent plasma capacitance values are quite small, on the order of a pF, and the effective resistances are fairly high MΩ – GΩ. Because of the small net capacitances, any parasitic capacitances associated with each circuit component may strongly influence the system's overall performance, so careful consideration should be made in any power system design.

Moreover, the effective resistance/capacitance model indicates a strong dependency on amplitude, but not very much dependence on frequency. Other than differences in the required voltage levels, similar impedance trends were observed for the un-gapped and gapped actuators. DBD plasma actuators are highly reactive devices, leading to large amounts of reactive power and motivating the need for impedance matching networks. However, conventional methods of impedance matching may become rather challenging, as the components required are large and not very common, especially since they must tolerate the kilovolts range of amplitudes needed to power DBD plasma actuators. Specialty custom-made components may be required.

In summary, this article provides some physical insight and scaling information for the electrical impedance behavior of various DBD actuators. With this information, it is hoped that future efforts may use this information to achieve enhanced power transfer by appropriate power system design.

Acknowledgments

This work was sponsored in part by the Air Force Office of Scientific Research, Grant #FA9550-09-1-0416.

References

[1]Moreau, E., "Airflow Control by Non-Thermal Plasma Actuators," *J. Phys. D: Appl. Phys.*, Vol. 40, 2007, pp. 605 – 636.

[2]Chen, Z., "Impedance Matching for One Atmosphere Uniform Glow Discharge Plasma (OAUGDP) Reactors," *IEEE Trans. Plasma Science*, Vol. 30, No. 5, 2002, pp. 1922 – 1930.

[3]Abrie, P. L., *The Design of Impedance-Matching Networks for Radio-Frequency and Microwave Amplifiers*, Artech House, Dedham, MA, 1985.

[4]Salem, M. M., Loiseau, J. F., and Held, B., "Impedance Matching for Optimization of Power Transfer in a Capacitively Excited RF Plasma Reactor," *Eur. Phys. J. AP*, Vol. 3, 1998, pp. 587 – 593.

[5]Singh, K. P., and Roy, S., "Physics of Plasma Actuator Operating in Atmospheric Air," *J. Appl. Phys. Let.*, Vol. 92, 2008, 111502.

[6]Orlov, D. M., Font, G. I., and Edelstein, D., "Characterization of Discharge Modes of Plasma Actuators," *AIAA Journal*, Vol. 46, No. 12, 2008, pp. 3142 – 3148.

[7]Chen, Z., "PSpice Simulation of One Atmosphere Uniform Glow Discharge Plasma (OAUGDP) Reactor Systems," *IEEE Trans. Plasma Science*, Vol. 31, No. 4, 2003, pp. 511 – 520.

[8]Enloe, C. L., McLaughlin, T. E., VanDyken, R. D., et al., "Mechanisms and Responses of a Single Dielectric Barrier Plasma Actuator: Plasma Morphology," *AIAA Journal*, Vol. 42, No. 3, 2004, pp. 589 – 594.